Molecules in intense xuv pulses: Beyond the dipole approximation in linearly and circularly polarized fields

M. Førre,[1] S. Selstø,[1] J. P. Hansen,[1] T. K. Kjeldsen,[2] and L. B. Madsen[2]
[1]*Department of Physics and Technology, University of Bergen, N-5007 Bergen, Norway*
[2]*Lundbeck Foundation Theoretical Center for Quantum System Research, Department of Physics and Astronomy, University of Aarhus, 8000 Aarhus, Denmark*
(Received 10 May 2007; published 26 September 2007)

The ionization dynamics of H_2^+ in an intense xuv laser pulse is studied beyond the dipole approximation in fields of linear and circular polarization. Our theoretical work shows distinct signatures of new ionization mechanisms and subsequent dynamics. Both low- and high-energy electrons emerge from the interaction to yield a characteristic and universal multilobe structure in the angular distributions which is uniquely linked to the initial molecular orientation. Each lobe is associated with its own characteristic electron dynamics. The emission spectra reveal processes that can be associated with single-center scattering, but show also clear evidence of two-center interference dynamics that can be explained by a simple two-center interference-diffraction model capturing the symmetry differences between $1\sigma_g$ and $1\sigma_u$ initial states.

DOI: 10.1103/PhysRevA.76.033415 PACS number(s): 33.80.Rv, 33.60.Cv, 42.50.Hz

Currently, major investments are made world-wide to develop new light sources based on the so-called free-electron laser (FEL) technology. Such sources will deliver radiation in pulses of femtosecond (10^{-15} s) duration with wavelengths ranging into the x-ray regime. The intensity will be high, exceeding the typical field strengths involved in keeping matter together. Intense xuv and x-ray sources are expected to be suitable for a range of applications, but the lack of experimental data on the behavior of matter under FEL pulses renders a detailed forecast difficult [1]. From a theory point of view, we expect the usual approximations that apply in the optical regime to break down, and to see, e.g., effects of radiation pressure. We are entering an unexplored regime which challenges the theoretical formulation and where predictions, in addition to their fundamental interest, may help in the planning and design of experimental techniques.

Recently, we showed, in high-intensity, high-frequency fields, that the angular differential ionization probability of H exhibits a characteristic nondipole multilobe structure, which includes a significant electron ejection in the direction opposite to the laser propagation direction [2]. In excited atomic systems, this lobe is predicted in the spectra at lower frequency, clearly exhibiting the sensitivity to the ratio between binding energy and laser frequency [3]. In [4,5] the geometrical dependence in the photoionization of H_2^+ by short, intense, high-frequency light pulses was studied within the dipole approximation, and recently the influence of nondipole effects on high-order harmonic generation spectra was investigated [6]. Previously, different aspects of strong-field nondipole dynamics in atoms were studied by several authors [7–11], including extension to a relativistic treatment (see, e.g., [12] and references therein).

In this work, we revisit the problem of ionization of matter by superintense laser fields beyond the dipole approximation, and address the question of how the simplest system exhibiting the chemical bond, H_2^+, responds to such extreme conditions. In particular, we investigate the differences between the response to a linearly and circularly polarized field. Likewise we address effects resulting from the symmetry of the molecular initial state, and illustrate such dependence by the use of $1\sigma_g$ and $1\sigma_u$ initial states, respectively. We predict the dynamics by numerical integration of the time-dependent Schrödinger equation (TDSE) [13], and explore the behavior of the electron as a strong external xuv field breaks the chemical bond. Some of the features characteristic to the ionization from a single center are retained, but important molecular effects appear which are partly related to the symmetry of the electronic initial state and which can partly be associated with interference between waves emitted from the two nuclei. The interference dynamics is explained in terms of a two-center interference-diffraction model.

Since the typical nuclear vibrational period is orders of magnitude longer than the pulse durations considered here, the nuclear degrees of freedom can be considered frozen during the dynamics. The nonrelativistic dynamics of H_2^+ in an intense electromagnetic field is then governed by the TDSE [atomic units (a.u.), $m_e=|e|=\hbar=a_0=1$, are used throughout], $i\partial_t\Psi=\left[\frac{1}{2}(\boldsymbol{p}+\boldsymbol{A})^2+V\right]\Psi$, with $\boldsymbol{A}(\boldsymbol{r},t)$ the space- and time-dependent vector potential, and V the two-center Coulomb potential, $V(\boldsymbol{r})=-1/|\boldsymbol{r}+\boldsymbol{R}/2|-1/|\boldsymbol{r}-\boldsymbol{R}/2|$, $\boldsymbol{R}$ being the internuclear vector. The field is sinusoidal $\sim\sin(\omega t-\boldsymbol{k}\cdot\boldsymbol{r}+\phi)$ and linearly or circularly polarized with ω the laser angular frequency and ϕ the carrier-envelope phase. The laser pulse has a sine-square profile with a central wavelength of 15 nm and a total pulse duration of 300 as, corresponding to six optical cycles. The field is intense with a peak intensity of 8.6×10^{19} W/cm^2, i.e., a peak electric field amplitude of $F_0=50$ a.u. The TDSE is solved with a split-step operator method [14,15]. In this approach the one-electron wave function is represented in spherical coordinates. The radial part is represented on a spatial grid and the angular part is expanded in spherical harmonics represented on an angular grid. The grid representation in all three coordinates makes the method very flexible. In particular, the method imposes no symmetry demands on the system under study, and accordingly, it is relatively straightforward to consider both linear and circular polarization as well as arbitrary molecular orientation (see, e.g., [16] and references therein for a discussion of the prob-

lems introduced by a circularly polarized field). Also, within the framework of a recently developed nondipole Kramers-Henneberger form of the light-matter interaction Hamiltonian, H_{KH} [13], it is possible to consider nondipole effects. The explicit form of this Hamiltonian is obtained by a unitary transformation of the conventional minimal-coupling Hamiltonian,

$$H_{\mathrm{KH}} = \frac{1}{2}p^2 + \frac{1}{2}A^2 + V(\boldsymbol{r}+\boldsymbol{\alpha}) + \frac{1}{2c^2}(\boldsymbol{A}\cdot\boldsymbol{p})^2 + \frac{1}{2c}[(\hat{\boldsymbol{k}}\cdot\boldsymbol{p})(\boldsymbol{A}\cdot\boldsymbol{p}) + (\boldsymbol{A}\cdot\boldsymbol{p})(\hat{\boldsymbol{k}}\cdot\boldsymbol{p})]. \quad (1)$$

Here, $\hat{\boldsymbol{k}}$ is a unit vector along the propagation direction, and $\boldsymbol{\alpha}(\boldsymbol{r},t)=\int_0^t \boldsymbol{A}(\boldsymbol{r},t')dt'$ the position relative to the laboratory frame of a classical free electron in the field. The angular differential ionization probability is calculated from the radial probability current flowing through a spherical boundary placed at some large distance $R_b \simeq 70a_0$, i.e.,

$$\frac{\partial P}{\partial \Omega} = \int_{t_0}^{T} \mathrm{Im}\,(r^2 \Psi^* \partial_r \Psi)|_{r=R_b} dt, \quad (2)$$

with t_0 the instant of time just after the end of the pulse and R_b large enough to ensure that no flux has passed it during the pulse. The final time T in Eq. (2) is such that all the outgoing flux has had time to pass R_b. The total size of the sphere used for the flux analysis is $150a_0$, and an absorbing boundary prevents unphysical reflections.

Figure 1 shows the probabilities for electron ejection in different directions and for different orientations [Figs. 1(a)–1(c)] of the molecule with respect to the electromagnetic pulse. The initial state is the $1\sigma_g$ and the field is linearly polarized. The angular distributions display a multilobe structure with a dominating electron ejection in the direction opposite to the pulse propagation direction independently of the orientation of the molecule with respect to the electromagnetic pulse. The insets in the upper right corners show the results when we neglect the spatial dependence of the laser pulse and use a field $\sim\sin(\omega t+\phi)$, i.e., work in the dipole approximation. Although the angular distributions are very similar in all three geometries, there is a clear difference between the dipole and nondipole results. We note that in ionization processes at high-frequency fields, both high-energy and low-energy electrons are emitted from the core and the relative portion of these electrons varies with the intensity of the field [13,15]. In Fig. 1, all structures with a component opposite to the propagation direction (i.e., II and III) consist of low-energy electrons ejected from the molecule as the radiation pressure decays, as we discuss further below. The structures parallel with the polarization direction (i.e., I) consist of high-energy electrons originating from one- and multiphoton ionization. In the dipole case (inset to the upper right) the structures II and III are missing, and a conventional dipole spectrum, with two lobes pointing along the polarization direction, is observed. Even though the underlying ionization dynamics is highly nonlinear, the gross structures in the dipole spectra in the present figures may be understood by considering simply the angular distributions

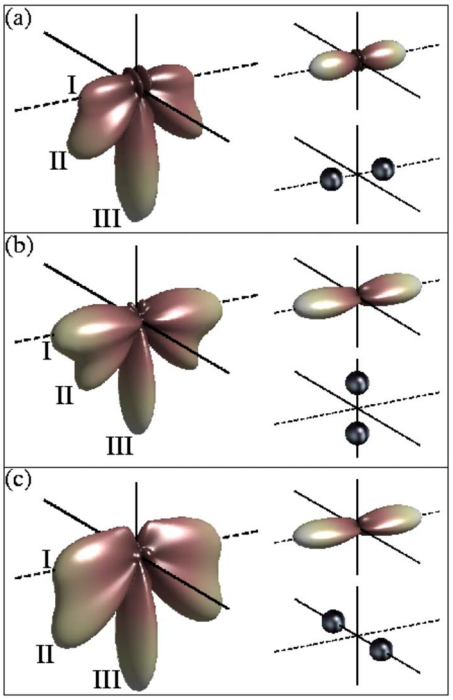

FIG. 1. (Color online) Electron angular distributions of H_2^+ after interaction with a linearly polarized six-cycle pulse with a wavelength of 15 nm and peak intensity 8.6×10^{19} W/cm^2, i.e., a peak electric field amplitude of $F_0=50$ a.u. The initial state is the $1\sigma_g$ electronic ground state at the mean internuclear distance $R=2a_0$. The pulse is propagating in the upward direction and the linear polarization axis is indicated by the dashed line. The data are averaged over the carrier-envelope phase difference. The insets in the lower right corners show the orientation of the molecule with respect to the pulse. Insets in the upper right corners show the results in the dipole approximation. The total ionization probabilities are $\simeq$0.24 and $\simeq$0.18 for the nondipole and dipole cases, respectively, nearly independent of geometry. The symbols I, II, and III denote features with the characteristic underlying ionization dynamics discussed in the text.

following single-photon absorption from the oriented initial state [5]. Deviations are due to higher-order processes including shake-off ionization by the short pulse. Accordingly, we shall not be much concerned with the dipole results in the following. They simply serve to highlight the signatures of nondipole effects.

When a bound electron is exposed to the very intense laser fields considered here, its wave function is displaced in the laser propagation direction due to the Lorentz force acting on it [2]. Hence the effect of the radiation pressure is that the electron accumulates momentum in the direction opposite to the propagation direction. This momentum component is necessarily small and has very little effect on the angular distribution stemming from the high-energy electrons. This explains the preservation of the dipole structure I in Fig. 1. On the other hand, low-energy electrons that are freed from the molecule by the electric field are effectively steered by the momentum component in the counterpropagating direction, giving rise to structure II in the spectra. The electrons that are building up the characteristic nondipole lobe (struc-

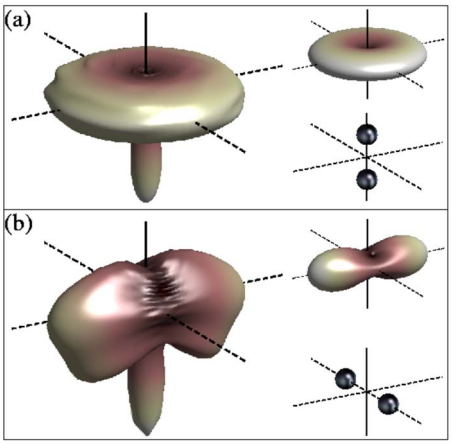

FIG. 2. (Color online) As Fig. 1, but for circular polarization with F_0=50 a.u. in each of the components of the circularly polarized field. The pulse propagates upwards and the plane of polarization is indicated by the dashed lines. The total ionization probabilities are in (a) 0.55 and 0.46 for the nondipole and dipole cases, respectively, and in (b) 0.52 and 0.43.

ture III) have two things in common [2]: They all have low energy, and they are not freed by the electric field alone. Instead, they are ionized as a result of an intimate interplay between magnetic, electric, and Coulomb forces acting all together during the pulse.

Figure 2 shows the corresponding angular distributions for a circularly polarized field and for two different geometries; again averaged over the carrier-envelope phase difference. In each panel we show the plane of polarization, the orientation of the molecule, and the nondipole and dipole angular distributions. The characteristic nondipole lobes in Figs. 2(a) and 2(b) pointing in the direction opposite to the propagation direction have the same origin as structure III in Fig. 1, i.e., they reflect the combined effect of the radiation pressure and the Coulomb field. For the orthogonal out-of-the-plane geometry (a) the distribution very much resembles the doughnutlike form stemming from the ionization from a single scattering center. In contrast, for the in-plane geometry (b) the electron is most likely ejected in the direction perpendicular to the internuclear axis. This spatial preference can be understood within a simple two-center interference-diffraction model where one assumes that the total outgoing wave consists of two outgoing waves originating from each of the two scattering centers [4],

$$\Psi_{\text{out}} = f_1(\Omega_1)\frac{e^{ik_e|\boldsymbol{r}+\boldsymbol{R}/2|}}{|\boldsymbol{r}+\boldsymbol{R}/2|} \pm f_2(\Omega_2)\frac{e^{ik_e|\boldsymbol{r}-\boldsymbol{R}/2|}}{|\boldsymbol{r}-\boldsymbol{R}/2|}, \tag{3}$$

where f_1 and f_2 are the two scattering amplitudes which we simply assume to be equal, but are dependent on pulse type and molecular orientation, and k_e is the momentum of the ejected electron. The "±" sign is determined by the gerade or ungerade symmetry of the initial state. For $r \gg R$ the differential ionization probability following this model can be brought into the simple form

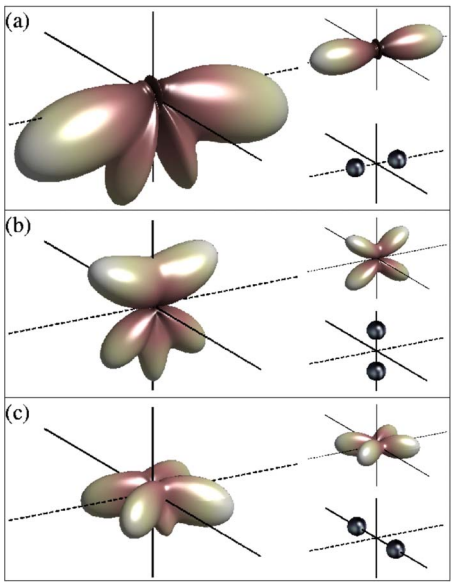

FIG. 3. (Color online) As Fig. 1, but for the $1\sigma_u$ initial state. The total ionization probabilities are in (a) 0.47 and 0.38 for the nondipole and dipole cases, respectively, in (b) 0.40 and 0.36, and in (c) 0.36 and 0.36.

$$\frac{\partial P}{\partial \Omega} \propto |f_1(\Omega)|^2[1 \pm \cos(k_e \hat{\boldsymbol{r}} \cdot \boldsymbol{R})]. \tag{4}$$

Care should be taken when using Eq. (4), as the ejected electron does not have a well defined momentum in the high-frequency, high-intensity limit [13]. However, for the case of a gerade initial state, Eq. (4) shows that for all directions with $\hat{\boldsymbol{r}} \cdot \boldsymbol{R} = 0$, the ionization yields from the two centers simply add together. For geometry (a) this means that the interference is constructive in all directions in the polarization plane, whereas for geometry (b) the two waves interfere constructively in the plane perpendicular to the internuclear axis.

Figures 3 and 4 show the differential ionization probability resulting from the ionization of an initial $1\sigma_u$ state in linearly and circularly polarized fields, respectively, and for different orientations of the molecule with respect to the electromagnetic pulse. The presence of the characteristic nondipole lobe also in these spectra emphasizes its general importance in the nondipole ionization dynamics. One striking feature is common for all geometries in Figs. 3 and 4: There is no electron ejection in the plane perpendicular to the internuclear axis. This stands in contrast to the situation described in Figs. 1 and 2 where the electron is likely to escape in all directions defined by this plane. Even the nondipole lobes in Figs. 3(a), 3(c), and 4(b) are cut into two pieces due to the symmetry plane. The whole difference can be attributed to the underlying antisymmetry of the initial $1\sigma_u$ state. In fact, the nodal plane is also fully understood within the model (4). Imposing the "−" sign, which reflects the ungerade symmetry of the initial state, the model shows that electron emittance in this plane is forbidden. This prohibition is maintained in the nondipole dynamics. Note that it is only in the case of Figs. 1(c) and 3(c) that reflection in the plane

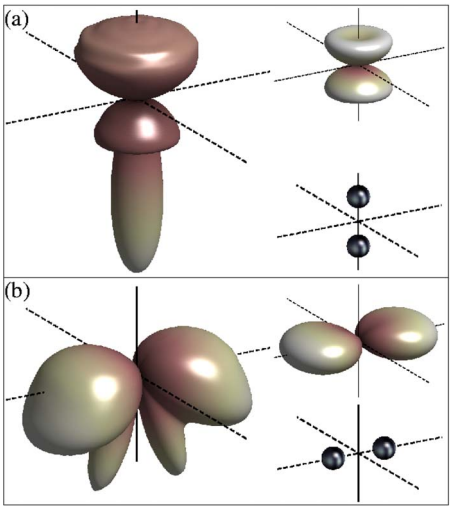

FIG. 4. (Color online) As Fig. 2, but for the $1\sigma_u$ initial state. The total ionization probabilities are in (a) 0.62 and 0.56 for the nondipole and dipole cases, respectively, and in (b) 0.69 and 0.55.

orthogonal to and midway between the nuclei represents an exact symmetry in both dipole and nondipole cases. Accordingly, only in this case is the nodal plane in Fig. 3(c) a strict formal necessity. In general, however, we find that the nondipole results tend to conserve the nodal structures of the dipole case.

In conclusion, we have carried out first principle nonperturbative calculations for the photoionization of H_2^+ by an intense xuv light source in an intensity and frequency regime where the spatial dependence of the laser field cannot be neglected. Clear evidence of both nondipole effects and two-center interference were identified in the differential probability distributions of the emitted photoelectron. A polarization independent nondipole lobe has been identified for the molecular system that, in general, and in clear contrast to the atomic case [2], cannot be illuminated by classical trajectory Monte Carlo (CTMC) simulations. The spectra from circular polarized light as well as from ungerade initial states turn out to depend strongly on the molecular orientation. The differences observed for different orientation and polarization indicate that future polarized FEL sources are suitable probes of molecular processes at the quantum level. The present results show what qualitatively new physics one can expect when matter interacts with very intense, high-energy FEL pulses. Thus the FEL facilities will not only be important as technology platforms, e.g., for structural imaging at the nano- and subnanoscale, but are also expected to expose signatures of new physical mechanisms as in the present case.

The present research was supported by the Norwegian Research Council through the NANOMAT program, the Nordic Research Board NordForsk, and the Danish Research Agency (Grant No. 2117-05-0081).

[1] H. Wabnitz *et al.*, Nature (London) **420**, 482 (2002).
[2] M. Førre, J. P. Hansen, L. Kocbach, S. Selstø, and L. B. Madsen, Phys. Rev. Lett. **97**, 043601 (2006).
[3] M. Førre, Phys. Rev. A **74**, 065401 (2006).
[4] S. Selstø, M. Førre, J. P. Hansen, and L. B. Madsen, Phys. Rev. Lett. **95**, 093002 (2005).
[5] S. Selstø, J. F. McCann, M. Førre, J. P. Hansen, and L. B. Madsen, Phys. Rev. A **73**, 033407 (2006).
[6] A. D. Bandrauk and H. Z. Lu, Phys. Rev. A **73**, 013412 (2006).
[7] A. Bugacov, M. Pont, and R. Shakeshaft, Phys. Rev. A **48**, R4027 (1993).
[8] N. J. Kylstra, R. A. Worthington, A. Patel, P. L. Knight, J. R. Vázquez de Aldana, and L. Roso, Phys. Rev. Lett. **85**, 1835 (2000).
[9] T. Mercouris, Y. Komninos, and C. A. Nicolaides, J. Phys. B **35**, 1439 (2002).
[10] K. J. Meharg, J. S. Parker, and K. T. Taylor, J. Phys. B **38**, 237 (2005).
[11] A. Staudt, C. H. Keitel, and J. S. Briggs, J. Phys. B **39**, 633 (2006).
[12] Y. I. Salamin, S. X. Hu, K. Z. Hatsagortsyan, and C. H. Keitel, Phys. Rep. **427**, 42 (2006).
[13] M. Førre, S. Selstø, J. P. Hansen, and L. B. Madsen, Phys. Rev. Lett. **95**, 043601 (2005).
[14] J. P. Hansen, T. Sørevik, and L. B. Madsen, Phys. Rev. A **68**, 031401(R) (2003).
[15] T. Birkeland, M. Førre, J. P. Hansen, and S. Selstø, J. Phys. B **37**, 4205 (2004).
[16] T. K. Kjeldsen, L. A. A. Nikolopoulos, and L. B. Madsen, Phys. Rev. A **75**, 063427 (2007).